universe

MDPI

Article

Influence of Finite Volume Effect on the Polyakov Quark–Meson Model

Niseem Magdy

Department of Physics, University of Illinois at Chicago, Chicago, IL 60607, USA; niseemm@gmail.com

Received: 20 March 2019; Accepted: 22 April 2019; Published: 24 April 2019

check for updates

Abstract: In the current work, we study the influence of a finite volume on $2+1$ $SU(3)$ Polyakov Quark–Meson model (PQM) order parameters, (fluctuations) correlations of conserved charges and the quark–hadron phase boundary. Our study of the PQM model order parameters and the (fluctuations) correlations of conserved charges indicates a sizable shift of the quark–hadron phase boundary to higher values of baryon chemical potential (μ_B) and temperature (T) for decreasing the system volume. The detailed study of such effect could have important implications for the extraction of the (fluctuations) correlations of conserved charges of the QCD phase diagram from heavy ion data.

Keywords: chiral lagrangian; quark confinement; quark-gluon plasma

1. Introduction

One of the major aims of the current heavy ion collisions research is to study the properties of the strongly interacting matter created in such collisions theoretically and experimentally. On the experimental level, many facilities have been designed to investigate the strongly interacting matter phase diagram such as Relativistic Heavy Ion Collider (RHIC) program [1], and the Large Hadron Collider (LHC) [2]. Different studies suggest that the strongly interacting matter phase transition from hadronic phase to quark–gluon plasma (QGP) phase be a smooth crossover at low density and high-temperature [3], and first-order phase transition at high density and low temperature [4,5]. Both smooth crossover and first-order phase transitions are expected to be connected by the critical endpoint (CEP), at which the phase transition is expected to be second order. One avenue to map out and study the QCD phase diagram is through the effective models such as the quark–meson (QM) model [6–8], the Nambu–Jona–Lasinio (NJL) model [9], and their Polyakov-loop extended versions [10].

Many studies have been devoted to investigating the QCD phase diagram, higher order moments and the thermodynamics of two- [11,12] and three-quark flavors [13] QM model and even PQM model with different Polyakov-loop potentials. The thermodynamic properties (pressure, the equation of state, the speed of sound, specific heat, trace anomaly, and the bulk viscosity) have been evaluated at finite and vanishing chemical potential [13,14].

The effect of a finite-volume on the strongly interacting matter has been widely studied [15–22]. Those studies include that finite volume has a strong effect on the transition temperature (T_c), the location of the critical endpoint and other thermodynamic properties. In PQM model, the transition temperature (T_c) shifted to large values as the volume decrease [21] and the location of the critical endpoint is shifted toward large μ and small T [17,18]. On the other hand, NJL [16] and PNJL [19] indicate that the transition temperature (T_c) shift to small values as the volume decrease and the location of the critical endpoint is shifted toward large μ and small T for 2 + 1 flavor and toward small μ and small T for 2 flavors.

In this work, we investigate the effect of the finite volumes on the PQM model order-parameters, phase-transition, and the conserved charges fluctuations and correlations. The present work is organized as follows. In Section 2, we give a brief overview of the PQM model. The PQM model calculations of the order-parameters, thermodynamic properties, and the conserved charges fluctuations and correlations are compared with the LQCD [23,24], and the influence of finite-volume effect on the PQM model conserved-quantities, baryon, charge, strangeness and their correlations are presented in Section 3. We conclude with a summary and an outlook in Section 4.

2. The Polyakov Quark–Meson (PQM) Model

The $SU(3)$ Quark–Meson model with $N_f = 2+1$ flavor quarks is coupled to Polyakov loop dynamics to formulate the Polyakov Quark–Meson (PQM) model [13]. The related Lagrangian is given as

$$\mathcal{L} = \mathcal{L}_{\text{chiral}} - \mathcal{U}(\phi, \phi^*, T), \tag{1}$$

where the chiral part of the Lagrangian, $\mathcal{L}_{\text{chiral}} = \mathcal{L}_{quark} + \mathcal{L}_{meson}$ has $SU(3)_L \times SU(3)_R$ symmetry [25,26]. The first part provides the fermionic sector, and the second part represents the mesonic contribution; both contributions are extensively discussed in Ref. [14].

The second term in Equation (1), $\mathcal{U}(\phi, \phi^*, T)$, represents the Polyakov-loop effective potential [27], which is expressed by using the dynamics of the thermal expectation value of a color traced Wilson loop in the temporal direction

$$\Phi(\vec{x}) = \frac{1}{N_c} \langle \mathcal{P}(\vec{x}) \rangle, \tag{2}$$

Then, the Polyakov-loop potential and its conjugate read:

$$\phi = (\text{Tr}_c\, \mathcal{P})/N_c, \tag{3}$$

$$\phi^* = (\text{Tr}_c\, \mathcal{P}^\dagger)/N_c, \tag{4}$$

where $\mathcal{P}$ is the Polyakov loop. This can be represented by a matrix in the color space [27]

$$\mathcal{P}(\vec{x}) = \mathcal{P}\text{exp}\left[i \int_0^\beta d\tau A_4(\vec{x}, \tau) \right], \tag{5}$$

where $\beta = 1/T$ is the inverse temperature and $A_4 = iA^0$ is called Polyakov gauge [27,28].

In the case of no quarks and zero quark chemical potential, $\phi = \phi^*$ and the Polyakov loop is recognized as an order parameter for the deconfinement phase-transition [29]. In the present work, we use Polyakov loop effective potential $U(\phi, \phi^*, T)$ as discussed in Refs. [29,30], but with a new dimensionless parameter K that helps us get a better agreement with the LQCD. Other Polyakov loop potentials [31,32] are also examined in various work. However, the particular selection made for this work does not affect the main conclusions of our work.

$$\frac{\mathcal{U}(\phi, \phi^*, T)}{T^4} = -\frac{B}{2}\phi\phi^* - \frac{a_1}{6}(\phi^3 + \phi^{*^3}) + \frac{a_2}{4}(\phi\phi^*)^2 - K\, ln[1 - 6\phi\phi^* + 4(\phi^3 + \phi^{*^3}) - 3(\phi\phi^*)^2], \tag{6}$$

where B and K are dimensionless parameters given as:

$$B = b_0 + b_1 \left(\frac{T_0}{T}\right) + b_2 \left(\frac{T_0}{T}\right)^2 + b_3 \left(\frac{T_0}{T}\right)^3, \tag{7}$$

$$K = k_1 \left(\frac{T_0}{T}\right) + k_2 \left(\frac{T_0}{T}\right)^2 + k_3 \left(\frac{T_0}{T}\right)^3 + k_4 \left(\frac{T_0}{T}\right)^4. \tag{8}$$

The mean field approximation is used following Refs. [14,33] to obtain the grand potential as:

$$\Omega(T, \mu_f) = U(\sigma_x, \sigma_y) + \mathcal{U}(\phi, \phi^*, T) + \Omega_{\bar{\psi}\psi}(T, \mu_f; \phi, \phi^*), \tag{9}$$

where σ_x and σ_y are the non-strange and strange chiral condensates, and the first term in Equation (9) is a purely mesonic potential expressed as:

$$\begin{aligned} U(\sigma_x, \sigma_y) &= \frac{m^2}{2}(\sigma_x^2 + \sigma_y^2) - h_x\sigma_x - h_y\sigma_y - \frac{c}{2\sqrt{2}}\sigma_x^2\sigma_y \\ &+ \frac{\lambda_1}{2}\sigma_x^2\sigma_y^2 + \frac{1}{8}(2\lambda_1 + \lambda_2)\sigma_x^4 + \frac{1}{4}(\lambda_1 + \lambda_2)\sigma_y^4. \end{aligned} \tag{10}$$

Here, m^2, h_x, h_y, λ_1, λ_2 and c are model parameters, as reported in Ref. [26]. The parameters values used in the current study are listed in Table 1. Different studies [34,35] indicate that extending the PQM model with the vector meson sector will help to accomplish better agreement with LQCD at $T < T_c$. Such correction is not included in this work and shall be discussed in future work.

The third term in Equation (9), $\Omega_{\bar{\psi}\psi}(T, \mu_f; \phi, \phi^*)$, which gives the quark and anti-quark contributions, can be shown as [13],

$$\begin{aligned} \Omega_{\bar{\psi}\psi}(T, \mu_f; \phi, \phi^*) &= -2T \sum_f \int \frac{d^3p}{(2\pi)^3} \\ &\left\{ \ln\left[1 + 3\left(\phi + \phi^* e^{-\frac{(E_f - \mu_f)}{T}}\right) e^{-\frac{(E_f - \mu_f)}{T}} + e^{-3\frac{(E_f - \mu_f)}{T}}\right] \right. \\ &\left. + \ln\left[1 + 3\left(\phi^* + \phi e^{-\frac{(E_f + \mu_f)}{T}}\right) e^{-\frac{(E_f + \mu_f)}{T}} + e^{-3\frac{(E_f + \mu_f)}{T}}\right] \right\}. \end{aligned} \tag{11}$$

where N gives the number of the quark flavors, $E_f = \sqrt{\vec{p}^2 + m_f^2}$ (the index f runs over different quark flavors (u, d and s)) is the dispersion relation, energy, of the valence quark and antiquark. Assuming degenerate light quarks, $q \equiv u, d$, then we can give the masses as follows:

$$m_q = g\frac{\sigma_x}{2}, \tag{12}$$

$$m_s = g\frac{\sigma_y}{\sqrt{2}}. \tag{13}$$

The quark chemical potentials μ_f are related to the baryon (μ_B), strange (μ_S) and charge (μ_Q) chemical potentials via the following transformations [36];

$$\begin{aligned}\mu_u &= \frac{\mu_B}{3} + \frac{2\mu_Q}{3}, \\ \mu_d &= \frac{\mu_B}{3} - \frac{\mu_Q}{3}, \\ \mu_s &= \frac{\mu_B}{3} - \frac{\mu_Q}{3} - \mu_S,\end{aligned}$$

The influences of a finite volume are introduced in the PQM model by following the approximate method illustrated in [19,37] via a lower momentum cut-off $p_{min}[GeV] = \pi/R[GeV] = \lambda$, where R is the length of a cubic volume. In this analysis, we study a simple situation (lower momentum cut-off). A full implementation of the finite volume would require decent consideration of the effects of the surface and curvature, as well as boundary conditions that are periodic for bosons and anti-periodic for fermions. This full implementation of the boundary conditions leads to an infinite sum over discrete momentum values.

The PQM model has a set of parameters, as discussed in Refs [26,30] and listed in Tables 1 and 2.

Table 1. Summary of the QM model parameters employed in the presented calculations.

c (MeV)	λ_1	m^2 (MeV^2)	λ_2	h_x (MeV^3)	h_y (MeV^3)
4807.84	1.40	$(342.52)^2$	46.48	$(120.73)^3$	$(336.41)^3$

Table 2. Summary of the Polyakov loop potential parameters employed in the presented calculations.

a_1	a_2	b_0	b_1	b_2	b_3
0.75	7.5	6.75	−1.95	2.625	−7.44
k_1	k_2	k_3	k_4		
0.30	0.25	0.24	0.20		

To estimate the model different parameters, σ_x, σ_y, ϕ and ϕ^*, we minimize the thermodynamic potential, Equation (9), with respect to σ_x, σ_y, ϕ and ϕ^*, which gives us a set of four equations of motion:

$$\frac{\partial\Omega}{\partial\sigma_x} = \frac{\partial\Omega}{\partial\sigma_y} = \frac{\partial\Omega}{\partial\phi} = \left.\frac{\partial\Omega}{\partial\phi^*}\right|_{min} = 0, \tag{14}$$

where $\sigma_x = \bar{\sigma_x}$, $\sigma_y = \bar{\sigma_y}$, $\phi = \bar{\phi}$ and $\phi^* = \bar{\phi}^*$ are the global minimum.

3. Results

In this section, we discuss our PQM model calculations using the parameters summarized in Tables 1 and 2 to illustrate the effect of finite volume on the model order parameters, phase transition and fluctuations/correlations of the conserved charges.

3.1. Order Parameters and Phase Transition

In the following, we present several calculations to illustrate the impacts of the finite volumes on the PQM model order parameters and the chiral phase transition.

Figure 1a–c shows the thermal dependence of the non-strange and strange chiral condensates (σ_x, σ_y) and Figure 1d–f shows the Polyakov loops (ϕ and ϕ^*) for different volume selections and different μ_B values. The upper panels show that both σ_x and σ_y increase as the system volume is decreased, with larger sensitivity for the non-strange chiral condensates (σ_x). The lower panels show very little if any, volume dependence for ϕ and ϕ^* at different μ_B.

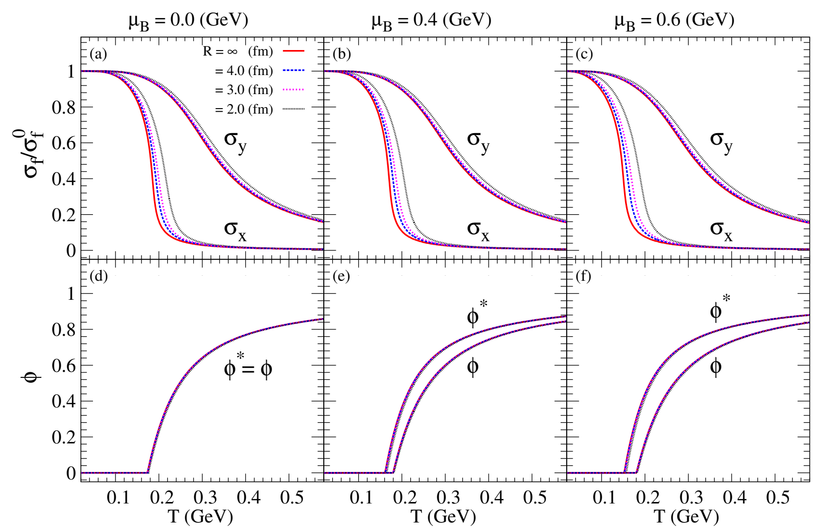

Figure 1. Temperature dependence of the: (non)strange chiral condensates (σ_x) σ_y (**a**–**c**); and the two Polyakov loops (ϕ, ϕ^*) (**d**–**f**) for several volume selections with μ_B = 0.0, 0.4 and 0.6 GeV.

As mentioned above, PQM model contains strange and non-strange chiral condensates, which reflect the chiral phase transitions. Using both chiral condensates, we can investigate the finite volume effects on the $SU(3)$ $2+1$ PQM model chiral phase transition via the normalized net-difference condensate $\Delta_{ls}(T)$, as defined in Ref. [38],

$$\Delta_{ls}(T) = \frac{\sigma_x - \frac{h_x}{h_y}\sigma_y}{\sigma_{x0} - \frac{h_x}{h_y}\sigma_{y0}}, \tag{15}$$

where h_x (h_y) are non-strange (strange) explicit symmetry breaking parameters.

Figure 2a–c shows the thermal dependence of the normalized net-difference condensate Δ_{ls} and Figure 2d–f shows the $d\Delta_{ls}/dT$ for different volume selections and different μ_B values. The upper panels indicate an increase in $\Delta_{ls}(T)$ as the system volume is decreased. The lower panels show that for fixed values of R and μ_B, the $d\Delta_{ls}/dT$ is peaking up at a specific point indicating the phase transition. The peak position is shifted toward lower temperature as the μ_B value increase.

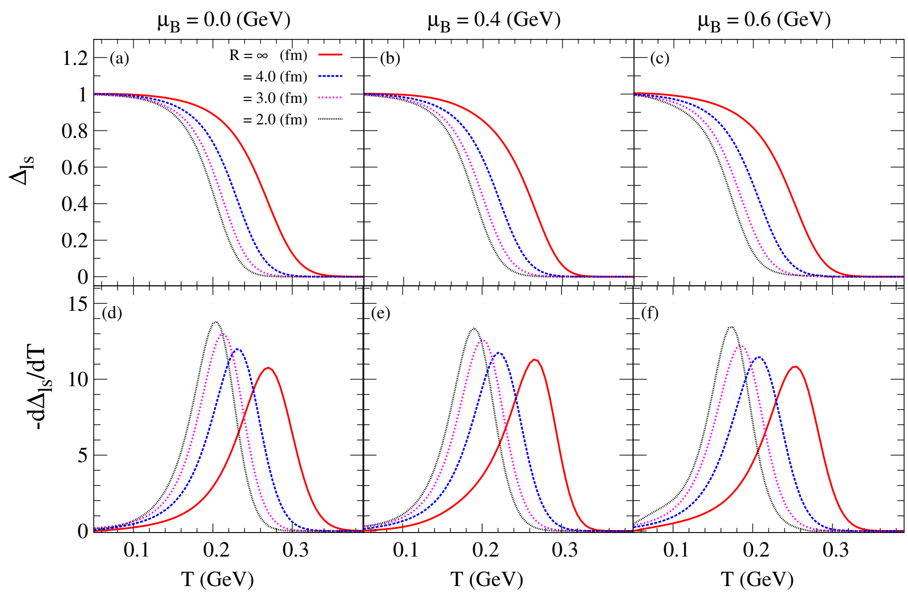

Figure 2. The same as in Figure 1 but for: the net-difference condensate (Δ_{ls}) (**a**–**c**); and $d\Delta_{ls}/dT$ (**d**–**f**).

The study of the phase diagram of the PQM model for at fixed volume could be done through mapping out the μ_B dependence of $\Delta_{q,s}(T)$. For a fixed R and μ_B values, $d\Delta_{ls}/dT$ will peak at a particular point expressing the phase transition. Therefore, the phase diagram can be studied by outlining such points for a wide range of baryon chemical potentials. Figure 3 illustrates the effects of finite volume on the phase diagram. The parameters T_c and μ_{Bc} represent the transition temperature at μ_B = 0.0 GeV and the transition chemical potential at low temperature, respectively, at $R = \infty$. Our calculations reveal that the PQM model phase diagram in the (μ_B, T)-plane, increases with decreasing the system volume. For the R = 2.0 (fm), the μ_B value at low temperature increased by about 30% and the T value at μ_B = 0.0 GeV increased by about 19% from them values at $R = \infty$ (fm).

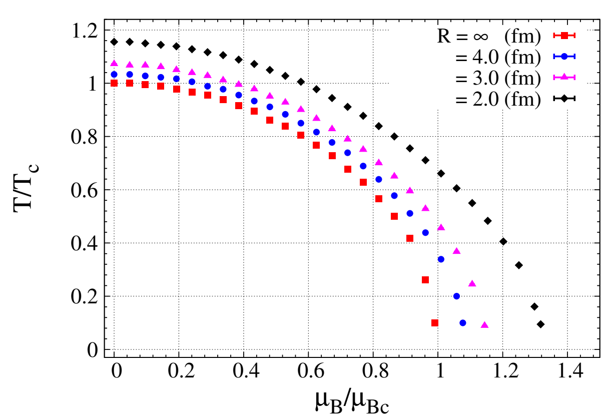

Figure 3. Chiral phase diagram for different volumes selections.

3.2. Fluctuations and Correlations of Conserved Charges

The thermodynamics quantities and (diagonal) off-diagonal susceptibilities can be determined by using the thermodynamic pressure as [24],

$$p = -\Omega(T, \mu_f), \tag{16}$$
$$s = dp/dT, \tag{17}$$
$$\epsilon = Ts - p, \tag{18}$$

$$\chi^{ijk}_{BQS} = \frac{\partial^{i+j+k}(p)}{\partial(\mu_B)^i \partial(\mu_Q)^j \partial(\mu_S)^k}. \tag{19}$$

where superscripts i, j and k run over integers that represent the derivatives orders. The indexes B, Q and S represent the conserved-quantities, baryon, charge, and strangeness, respectively. Equation (19) illustrates the dependence of the (fluctuations) correlations of conserved charges on the temperature, chemical potential, and system volume. The susceptibilities evaluated first by computing the thermodynamic potential at vanishing μ_f and then expand the scaled thermodynamic potential in a Taylor series around $\mu_f/T = 0$.

Before addressing the system volume effect, it is informative to contrast the PQM model thermodynamics quantities and (diagonal) off-diagonal susceptibilities calculations for ($\mu_B = 0$ and $R = \infty$), to similar results from LQCD calculations [23,24]. Such comparisons are presented in Figures 4 and 5, which indicate a good agreement between the PQM model and LQCD [23,24]. These comparisons could be improved spatially at low temperature by including the vector mesons sector to the PQM model. We discussed the influence of the finite volume on the model thermodynamics quantities in our previous study [21].

Figure 6 displays the temperature dependence of the normalized conserved-fluctuations, baryon (χ_{BB}), charge (χ_{QQ}) and strangeness (χ_{SS}), respectively. The results are presented for several volume selections at three μ_B values, $\mu_B = 0.0$, 0.4 and 0.6 GeV. Our results indicate that the normalized fluctuations decrease with the volume, which quickly trends towards the infinite volume value at high temperature. The non-strange susceptibilities (χ^2_{BB} and χ^2_{QQ}) shows a higher sensitivity to the volume change more than the strange susceptibility (χ^2_{SS}). This weak sensitivity to the volume change of the strange quantities could be driving from the large mass of the strange quark.

Figure 7 shows the temperature dependence of the off-diagonal susceptibilities, χ^2_{BQ}, χ^2_{BS} and χ^2_{SQ} for several volume selections and different μ_B values. The net baryons show a high correlation to the net charge and less correlation to the net strange. Our results indicate that the normalized correlations decrease with the volume which quickly trends towards the infinite volume value at high temperature. In addition, the non-strange correlation (χ_{BQ}) show a higher sensitivity to the volume change.

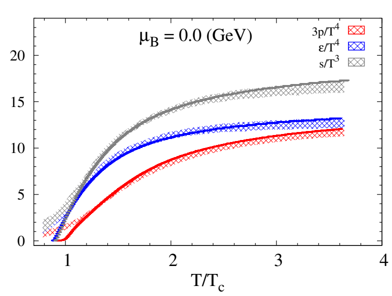

Figure 4. Comparison of the PQM model pressure density, energy density and entropy to results from LQCD. The comparisons are made for μ_B = 0.0 GeV; the lines indicate the PQM model calculations and the shaded areas indicate LQCD results from Ref. [23].

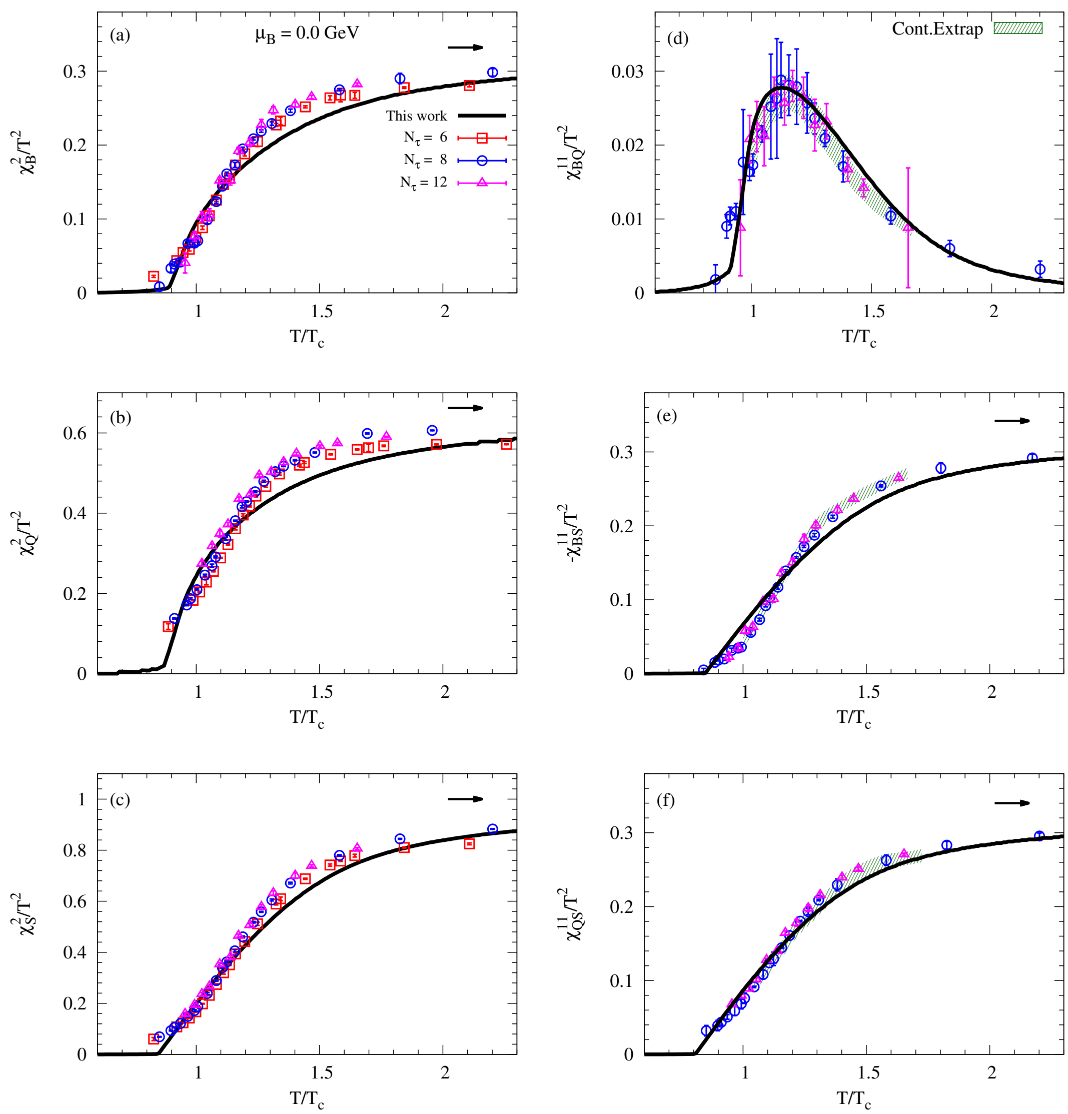

Figure 5. The thermal behavior of PQM model conserved charges fluctuation (**a**–**c**); and correlation (**d**–**f**) are compared with the same quantities obtained from the LQCD (symbols). The comparisons are made for $\mu_B = 0$. The LQCD conserved charges fluctuation (**a**–**c**) and correlation (**d**–**f**) are taken from Ref. [24] (Tables III, IV and V).

In addition, the temperature dependence of the higher order baryon susceptibilities χ_B^n (n = 4, 6 and 8) for different volume selections at μ_B values, μ_B = 0.0, 0.4 and 0.6 GeV are shown in Figure 8. The nth-order susceptibilities decrease with the volume selections, and, for $n = 6, 8$ they start to peak around the transition temperature T_c. In addition, we observe a stronger oscillation in all higher harmonics as we increase the μ_B values.

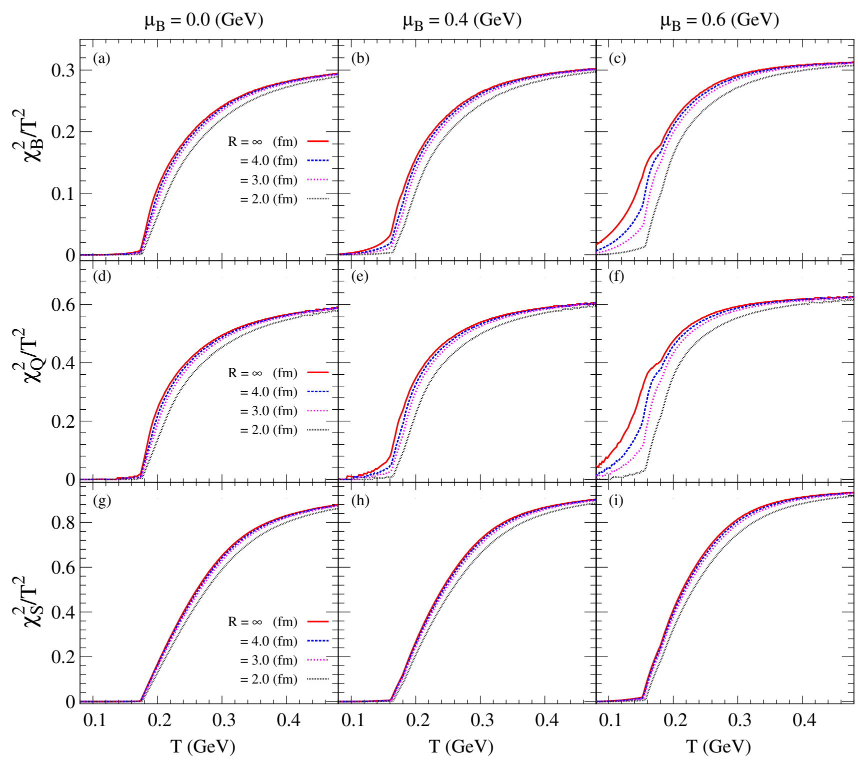

Figure 6. The thermal behavior of the normalized diagonal susceptibilities, χ^2_{BB}, χ^2_{QQ} and χ^2_{SS}, for several volume selections at μ_B = 0.0, 0.4 and 0.6 GeV.

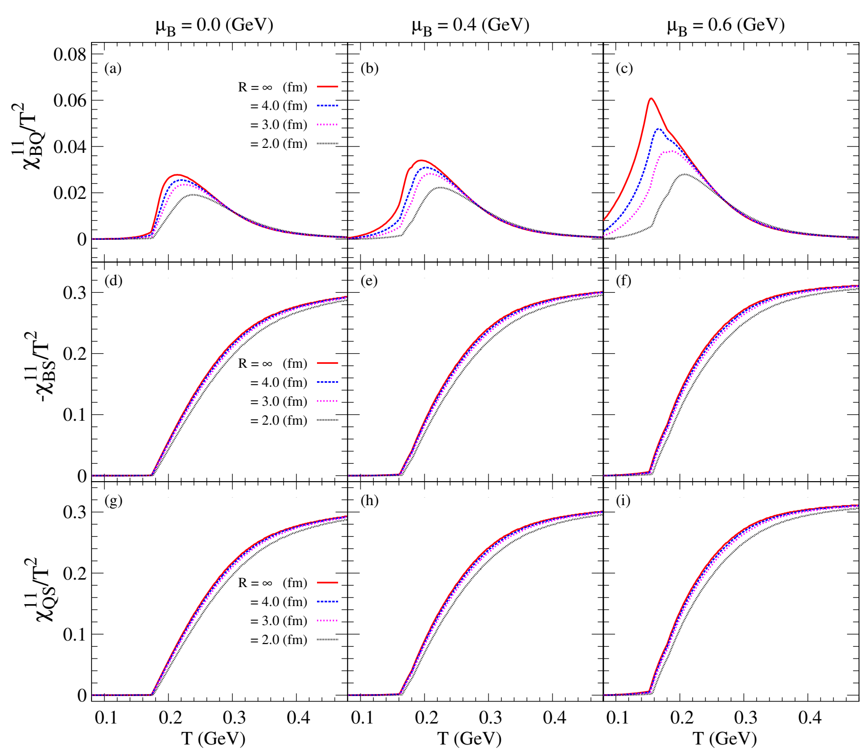

Figure 7. The thermal behavior of the normalized off-diagonal susceptibilities, χ^{11}_{BQ}, χ^{11}_{BS} and χ^{11}_{QS}, for several volume selections at μ_B = 0.0, 0.4 and 0.6 GeV.

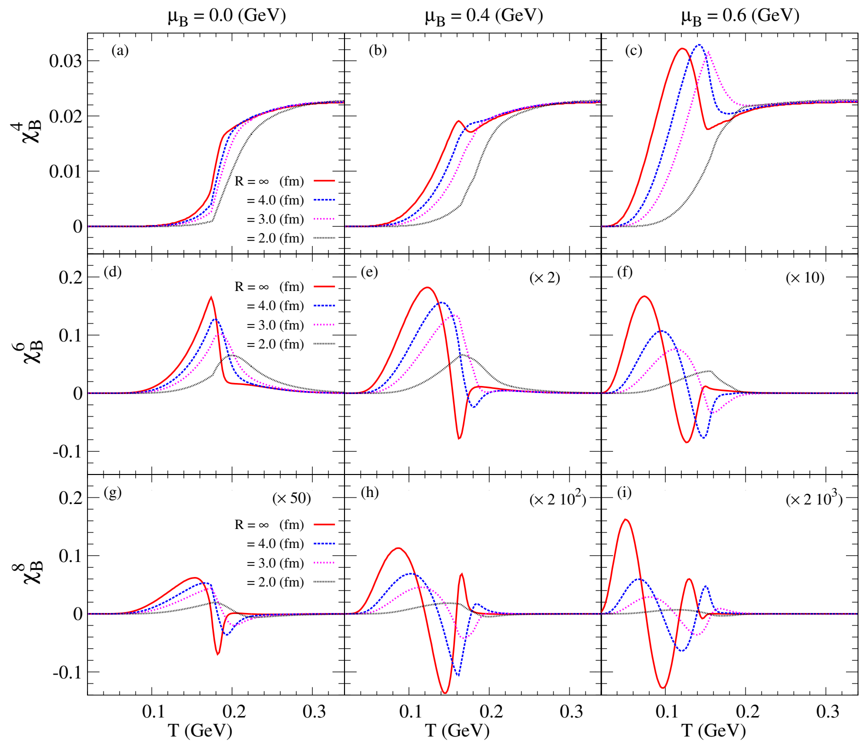

Figure 8. The thermal behavior of the higher order susceptibilities, χ_B^4, χ_B^6 and χ_B^8, for several volume selections at μ_B = 0.0, 0.4 and 0.6 GeV.

4. Conclusions

In this work, we have used the $2+1$ $SU(3)$ Polyakov Quark–Meson model (PQM) framework to study the properties of the QCD medium produced at finite volume in heavy ion collisions. This model framework provides several conserved-quantities, baryon, charge, and strangeness, which compare well with those obtained in LQCD calculations for vanishing μ_B. Our calculations indicate that the conserved-quantities (χ_{BQS}^{ijk}) are significantly influenced by finite volume effects. The calculated conserved-quantities decrease with the volume, which quickly trends towards the infinite volume value at high temperature. In addition, the non-strange quantities show a higher sensitivity to the volume change more than the strange once. Finally, PQM model conserved-quantities suggests that the quark–hadron phase boundary is shifted to higher values of μ_B and T with decreasing system volume.

Funding: This work is supported by the US Department of Energy under contract DE-FG02-94ER40865.

Acknowledgments: The author thanks Emily E. Racow for her great input.

Conflicts of Interest: The author declare no conflict of interest.

References

1. Fachini, P. Experimental highlights of the RHIC program. In Proceedings of the PARTICLES AND FIELDS: X Mexican Workshop on Particles and Fields, Morelia, Mexico, 6–12 November 2005; AIP: New York, NY, USA, 2006; pp. 62–75.
2. Monteno, M. The physics programme of the ALICE experiment at the LHC. *Nucl. Phys. A* **2007**, *782*, 283–290. [CrossRef]

3. Aoki, Y.; Endrodi, G.; Fodor, Z.; Katz, S.D.; Szabo, K.K. The Order of the quantum chromodynamics transition predicted by the standard model of particle physics. *Nature* **2006**, *443*, 675–678. [CrossRef]
4. Ejiri, S. Canonical partition function and finite density phase transition in lattice QCD. *Phys. Rev. D* **2008**, *78*, 074507. [CrossRef]
5. Pisarski, R.D.; Wilczek, F. Remarks on the Chiral Phase Transition in Chromodynamics. *Phys. Rev. D* **1984**, *29*, 338. [CrossRef]
6. Lee, B.W. *Chiral Dynamics*; Gordon and Breach: New York, NY, USA, 1972; Volume B591, 129p.
7. Kovacs, P.; Szep, Z. The critical surface of the $SU(3)_L \times SU(3)_R$ chiral quark model at non-zero baryon density. *Phys. Rev. D* **2007**, *75*, 025015. [CrossRef]
8. Kovacs, P.; Szep, Z. Influence of the isospin and hypercharge chemical potentials on the location of the CEP in the $\mu_B - T$ phase diagram of the $SU(3)_L \times SU(3)_R$ chiral quark model. *Phys. Rev. D* **2008**, *77*, 065016. [CrossRef]
9. Nambu, Y.; Jona-Lasinio, G. Dynamical Model of Elementary Particles Based on an Analogy with Superconductivity. II. *Phys. Rev.* **1961**, *124*, 246.
10. Fukushima, K. Chiral effective model with the Polyakov loop. *Phys. Lett. B* **2004**, *591*, 277–284. [CrossRef]
11. Kahara, T.; Tuominen, K. Degrees of freedom and the phase transitions of two flavor QCD. *Phys. Rev. D* **2008**, *78*, 034015. [CrossRef]
12. Wambach, J.; Schaefer, B.J.; Wagner, M. QCD Thermodynamics: Confronting the Polyakov–Quark–Meson Model with Lattice QCD. *Acta Phys. Polon. Suppl.* **2010**, *3*, 691–700.
13. Schaefer, B.J.; Wagner, M. On the QCD phase structure from effective models. *Prog. Part. Nucl. Phys.* **2009**, *62*, 381–385. [CrossRef]
14. Mao, H.; Jin, J.; Huang, M. Phase diagram and thermodynamics of the Polyakov linear sigma model with three quark flavors. *J. Phys. G Nucl. Part. Phys.* **2010**, *37*, 035001. [CrossRef]
15. Fisher, M.E.; Barber, M.N. Scaling Theory for Finite-Size Effects in the Critical Region. *Phys. Rev. Lett.* **1972**, *28*, 1516–1519. [CrossRef]
16. Abreu, L.M.; Gomes, M.; da Silva, A.J. Finite-size effects on the phase structure of the Nambu-Jona-Lasinio model. *Phys. Lett. B* **2006**, *642*, 551–562. [CrossRef]
17. Palhares, L.F.; Fraga, E.S.; Kodama, T. Chiral transition in a finite system and possible use of finite size scaling in relativistic heavy ion collisions. *J. Phys. G Nucl. Part. Phys.* **2011**, *38*, 085101. [CrossRef]
18. Fraga, E.S.; Palhares, L.F.; Sorensen, P. Finite-size scaling as a tool in the search for the QCD critical point in heavy ion data. *Phys. Rev. C* **2011**, *84*, 011903. [CrossRef]
19. Bhattacharyya, A.; Deb, P.; Ghosh, S.K.; Ray, R.; Sur, S. Thermodynamic Properties of Strongly Interacting Matter in Finite Volume using Polyakov-Nambu-Jona-Lasinio Model. *Phys. Rev. D* **2013**, *87*, 054009. [CrossRef]
20. Bhattacharyya, A.; Ray, R.; Sur, S. Fluctuation of strongly interacting matter in the Polyakov–Nambu–Jona-Lasinio model in a finite volume. *Phys. Rev. D* **2015**, *91*, 051501. [CrossRef]
21. Magdy, N.; Csanád, M.; Lacey, R.A. Influence of finite volume and magnetic field effects on the QCD phase diagram. *J. Phys. G Nucl. Part. Phys.* **2017**, *44*, 025101. [CrossRef]
22. Almasi, G.; Pisarski, R.; Skokov, V. Volume dependence of baryon number cumulants and their ratios. *Phys. Rev. D* **2017**, *95*, 056015. [CrossRef]
23. Borsanyi, S.; Fodor, Z.; Hoelbling, C.; Katz, S.D.; Krieg, S.; Szabo, K.K. Full result for the QCD equation of state with $2+1$ flavors. *Phys. Lett. B* **2014**, *730*, 99–104. [CrossRef]
24. Bazavov, A.; Bhattacharya, T.; DeTar, C.E.; Ding, H.T.; Gottlieb, S.; Gupta, R.; Hegde, P.; Heller, U.M.; Karsch, F.; Laermann, E.; et al. Fluctuations and Correlations of net baryon number, electric charge, and strangeness: A comparison of lattice QCD results with the hadron resonance gas model. *Phys. Rev. D* **2012**, *86*, 034509. [CrossRef]
25. Lenaghan, J.T.; Rischke, D.H.; Schaffner-Bielich, J. Chiral symmetry restoration at nonzero temperature in the $SU(3)_L \times SU(3)_R$ linear sigma model. *Phys. Rev. D* **2000**, *62*, 085008. [CrossRef]
26. Schaefer, B.J.; Wagner, M. The Three-flavor chiral phase structure in hot and dense QCD matter. *Phys. Rev. D* **2009**, *79*, 014018. [CrossRef]

27. Polyakov, A.M. Thermal Properties of Gauge Fields and Quark Liberation. *Phys. Lett. B* **1978**, *72*, 477–480. [CrossRef]
28. Susskind, L. Lattice Models of Quark Confinement at High Temperature. *Phys. Rev. D* **1979**, *20*, 2610–2618. [CrossRef]
29. Ratti, C.; Thaler, M.A.; Weise, W. Phases of QCD: Lattice thermodynamics and a field theoretical model. *Phys. Rev. D* **2006**, *73*, 014019. [CrossRef]
30. Ghosh, S.K.; Mukherjee, T.K.; Mustafa, M.G.; Ray, R. PNJL model with a Van der Monde term. *Phys. Rev. D* **2008**, *77*, 094024. [CrossRef]
31. Haas, L.M.; Stiele, R.; Braun, J.; Pawlowski, J.M.; Schaffner-Bielich, J. Improved Polyakov-loop potential for effective models from functional calculations. *Phys. Rev. D* **2013**, *87*, 076004. [CrossRef]
32. Schaefer, B.J.; Wagner, M.; Wambach, J. QCD thermodynamics with effective models. *PoS* **2009**, *CPOD2009*, 017.
33. Tawfik, A.; Magdy, N.; Diab, A. Polyakov linear SU(3) σ model: Features of higher-order moments in a dense and thermal hadronic medium. *Phys. Rev. C* **2014**, *89*, 055210. [CrossRef]
34. Kovács, P.; Wolf, G. Chiral phase transition scenarios from the vector meson extended Polyakov quark meson model. *arXiv* **2015**, arXiv:1507.02064
35. Kovács, P.; Szép, Z.; Wolf, G. Existence of the critical endpoint in the vector meson extended linear sigma model. *Phys. Rev. D* **2016**, *93*, 114014. [CrossRef]
36. Fu, W.j. Fluctuations and correlations of hot QCD matter in an external magnetic field. *Phys. Rev. D* **2013**, *88*, 014009. [CrossRef]
37. Bhattacharyya, A.; Ray, R.; Samanta, S.; Sur, S. Thermodynamics and fluctuations of conserved charges in a hadron resonance gas model in a finite volume. *Phys. Rev. C* **2015**, *91*, 041901. [CrossRef]
38. Schaefer, B.J.; Wagner, M.; Wambach, J. Thermodynamics of (2 + 1)-flavor QCD: Confronting Models with Lattice Studies. *Phys. Rev. D* **2010**, *81*, 074013. [CrossRef]